Lung motion modelisation with deformable registration: non-linearity and hysteresis estimation and analysis

1 Introduction

Respiratory motion has been modeled in a variety of ways for different purposes. The most common models use either phase, amplitude, or both, and describe the motion of either a single point or a surrogate signal. Accurate motion modeling within the lung is an important consideration in different clinical application. In radiation therapy for example, for lung cancer patients treatment planning purposes, the motion is assessed for determination of planning margins as well as 4D optimization and new delivery adaptations. A precise modeling of pulmonary volume requires a considerable internal detail which is now available mainly thanks to medical image modalities like four-dimensional computed tomography (4D-CT) and fast magnetic resonance imaging (MRI). 4D-CT images are one of the solutions proposed in lung cancer radiotherapy treatment to deal with respiratory movement, but they must be associated to new medical imaging analysis tools. Using a motion model constructed from 4D-CT using deformable registration, the goal of this study is to follow both lung and tumor displacements and deformations during free breathing in order to extract physiological parameters like nonlinearity and hysteresis of motion.

2 Material and methods

2.1 4D-CT acquisition

4D-CT was acquired using a 4-slice fan-beam CT scanner (GE Lightspeed QX/i; GE Heathcare Technologies, Waukesha, WI), and a respiratory surrogate (Real-time Position Management; Varian Medical Systems, Palo Alto, CA). A complete description of the process is described in Rietzel et al. [1]. We consider 4D-CT scans for three patients treated in radiotherapy for lung cancer. 3D-CT images of the 4D-CT have an in-plane spatial resolution of 512×512, between 88 and 120 slices, and a voxel size of $0.977 \times 0.977 \times 2.5\ \mathrm{mm}^3$.

2.2 Motion model construction

Deformable image registration is an important topic in medical imaging, with direct application to radiotherapy. In this work the motion model was constructed from vector fields computed using an optical flow like algorithm (the "demons" algorithm [2]): similarity measure is SSD (sum of square differences), gaussian regularization. The 4D-CT scans are composed of ten 3D-CT images, numbered from 0 to 9. Image I_5 is the end-exhale image, and I_0 is the end-inhale 3D-CT image. I_1, I_2, I_3, I_4 are successive expiration states and I_6, I_7, I_8, I_9 are the successive inspiration states. The states are cyclic, such that I_0 follows I_9. From n images there are $\frac{n!}{(n-2)!}$ possible pairwise registrations. Although the deformation fields could be computed for all pairs, we would prefer to use fewer registrations to compute the model. The motion model was built by applying deformable registration between the reference image and all the other phases of the 4D-CT. For example, considering I_5 as reference, we compute U_{50}, U_{51}, $\cdots$, U_{59}, and then we compute U_{05}, U_{15}, $\cdots$, U_{95}. Thus, the model generated is comprised of eighteen deformable fields. Given these eighteen fields, a deformation field between arbitrary states can be generated by composition of only two vector fields. For example, the deformation field U_{13} is calculated as $U_{13} = U_{15} \circ U_{53}$.

2.3 Motion model evaluation

Control points validation For each patient, about 60 landmark points were manually identified by an expert within the lung of the end-inhale image of the 4D-CT. Then, two additional expert observers identified corresponding landmark points on all other 4D-CT phases. The mean distance between observers was 1.9 mm, and the standard deviation was 2.0 mm. For each landmark and for each phase, a composite reference location was obtained by calculating the mean value of the observer positions. These reference locations are used for validation. The model accuracy is estimated by computing the distances between the reference landmark locations and the estimated locations generated using the deformation fields. For example, given a deformation field U_{XY}, and p_X a reference location in I_X, then its estimate in I_Y is $\boldsymbol{p}'_Y = \boldsymbol{p}_X + U_{XY}(\boldsymbol{p}_X)$. The accuracy of this estimation is determined by computing the distances between $\boldsymbol{p}'_Y$ and the reference position $\boldsymbol{p}_Y$. The accuracy for U_{XY} is determined from the mean and standard deviation of these distances over the complete set of landmark points.

Consistency The consistency of a deformation field U_{XY} is evaluated by computing the mean and standard deviation of the displacement vector norms of the composite deformation field $U_{XY} \circ U_{YX}$. It is usually computed from four vector fields: $U_{X5} \circ U_{5Y} \circ U_{Y5} \circ U_{5X}$. Only two vector fields are required when $Y = X \pm 1$. If the model was consistent, the composed vector field would be zero everywhere.

2.4 Lung point trajectories

Building the trajectories A deformation field contains a displacement vector for each point, which describes the distance to the correspondence in the other image. Starting from the reference image I_5, we can therefore compute the trajectory of any point through the entire free-breathing cycle. If $\boldsymbol{p}_5$ is a point in image I_5, its correspondence $\boldsymbol{p}_Y$ in image I_Y is computed as $\boldsymbol{p}_Y = \boldsymbol{p}_5 + U_{5Y}(\boldsymbol{p}_5)$. Given the position of the point at all breathing states, we have a complete trajectory. Between p_X and p_{X+1} we will assume that the trajectory follows a straight line, and that it travels at constant velocity. This assumption is valid if the 4D-CT has sufficient temporal resolution. Thus, the trajectory is a piecewise linear closed curve, and is described by $T_p : \Omega_\Phi \rightarrow \mathbb{R}^3$, where Ω_Φ is the set of all possible states. For states $\Phi, \Phi \in [X, X+1]$, between X and $X+1$, the trajectory is given as:

$$T_{\boldsymbol{p}}(\Phi) = T_{\boldsymbol{p}}(X) + \lambda_\Phi U_{XX+1}(\boldsymbol{p}), \tag{1}$$

where $\lambda_\Phi = \Phi - X$, $\lambda_\Phi \in [0, 1]$. The parameter λ_Φ models trajectories between breathing phases successive 4D-CT phases. For example, one may relate parameter λ_Φ to a breathing model cycle such as the one proposed by Lujan et al. [3], or to the tidal volume and its temporal derivative in the 5D model proposed by Low et al. [4]. As mentioned in [4], however, the breathing motion is very complex and is not well modeled as a simple function of time. Ideally, a priori patient specific physiological information would be needed to simulate the temporal behavior of points trajectories during breathing. Each trajectory is related to an origin displacement in state 5, which is considered to be the most reproducible state of the free-breathing cycle [5]. Figure 1 illustrates the trajectories of two lungs points with different behaviour during the free breathing cycle: in blue the path through exhalation and in green the path through inhalation.

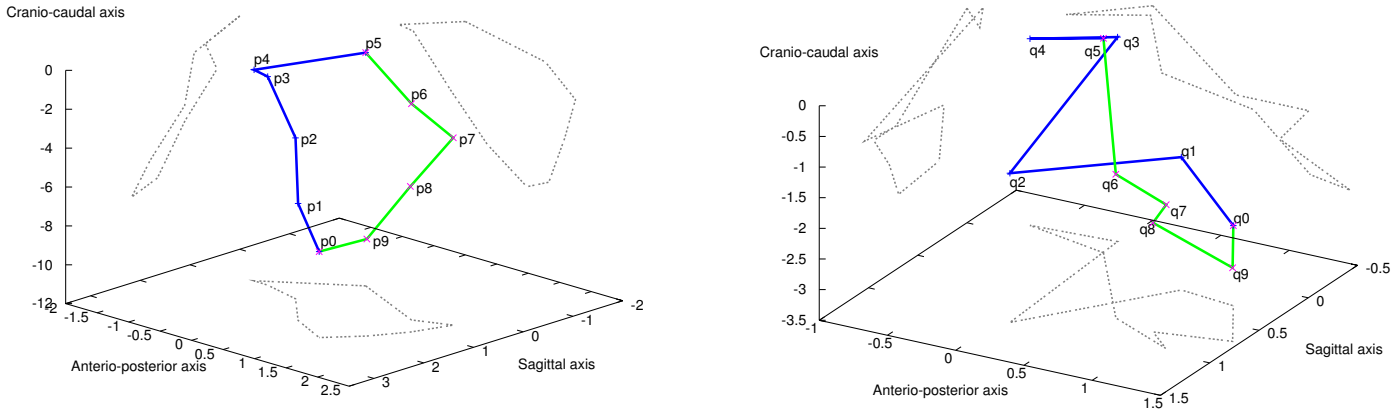

Figure 1: Trajectories of two lung points with different motion behaviour. $\boldsymbol{p}_X$, $\boldsymbol{q}_X$ denote point positions at different X states, $X \in \{0, 1, ..., 9\}$, of the free-breathing cycle. Projections of the trajectory on the transversal, sagittal and coronal planes are also illustrated.

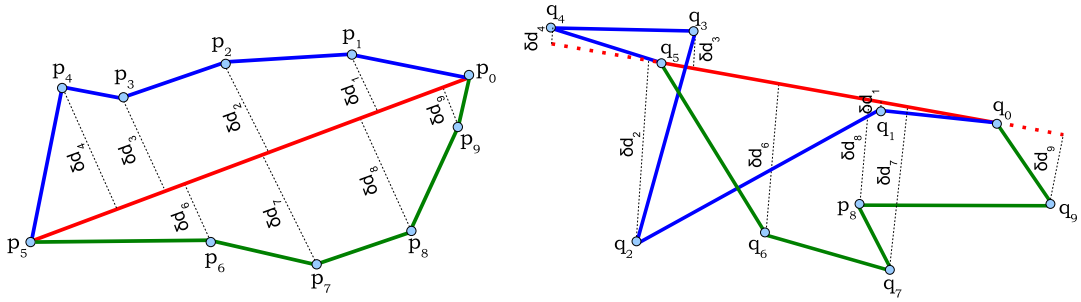

Figure 2: Two 2D illustrations of non-linearity evaluation for two points trajectories. In red, the straight line trajectory of point $\boldsymbol{p}_5$ estimated only between end-exhale and end-inhale phase; in blue, exhalation trajectoryn; in green, inhalation trajectory. δ_X denotes the distance between lung point position and the straight line trajectory.

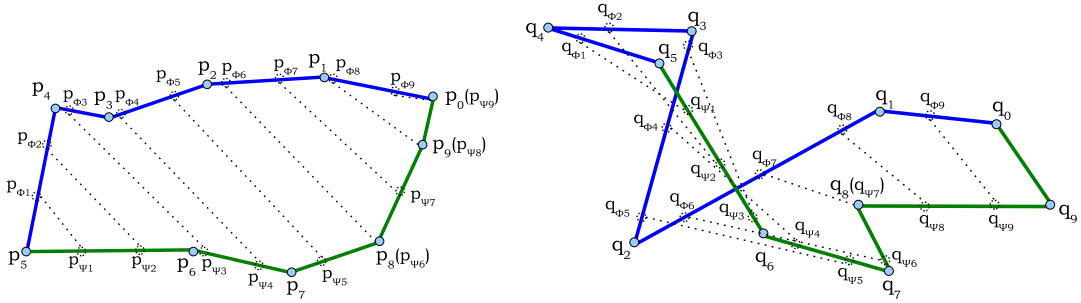

Figure 3: Two 2D illustrations of hysteresis computation for two different lung points, $\boldsymbol{p}$ and $\boldsymbol{q}$, starting from state 5 point positions and considering a sequence of 9 equal distant points ($\boldsymbol{p}_{\Phi_1}$, ..., $\boldsymbol{p}_{\Phi_9}$, respectively $\boldsymbol{q}_{\Phi_1}$,..., $\boldsymbol{q}_{\Phi_9}$) positions over exhalation trajectory and 9 equal distant points ($\boldsymbol{p}_{\Psi_1}$,..., $\boldsymbol{p}_{\Psi_9}$, respectively $\boldsymbol{q}_{\Psi_1}$, ..., $\boldsymbol{q}_{\Psi_9}$) over inhalation trajectory.

Motion non-linearity For each lung point, at each state X, we computed the distance $\delta_X(\boldsymbol{p})$, $\delta_X(\boldsymbol{p}) = d(\boldsymbol{p}_X, T_L(\boldsymbol{p}))$ to the straight line trajectory $T_L(p)$. Figure 2 illustrates in 2D the computation of distances to straight line trajectories for two lung points points $\boldsymbol{p}$ and $\boldsymbol{q}$. We evaluated the non-linearity of the lung point trajectories for six cranio-caudal regions. The first region (R_1) is composed of lungs points situated from 0% to 10% of H_p; the four (R_2, R_3, R_4, R_5) following regions are each composed of 20% and the last region (R_6) contains the last 10% of lung points.

Motion hysteresis The hysteresis was defined as the maximum distance between inhalation and exhalation trajectories [6]. The point trajectory defined in equation 1 is a non-planar polygonal curve. Computing hysteresis between inhalation and exhalation trajectories comes down to calculate the maximum distance between inhalation polygonal curve and exhalation polygonal curve. Let $L_{exh}(\boldsymbol{p})$ be the length of a point trajectory $\boldsymbol{p}$ over exhalation and let $L_{inh}(\boldsymbol{p})$ be its length over inhalation. Starting from $\boldsymbol{p}_5$, the point's position in phase 5, we construct a sequence of points along the exhale trajectory, $\boldsymbol{p}_{\Phi_1}$, $\boldsymbol{p}_{\Phi_2}$, ...$\boldsymbol{p}_{\Phi_n}$, such that the trajectory length between two successive point positions is constant. Then, we construct a similar sequence, starting from $\boldsymbol{p}_5$ along the inhale trajectory: $\boldsymbol{p}_5$, $\boldsymbol{p}_{\Psi_1}$, $\boldsymbol{p}_{\Psi_2}$,...$\boldsymbol{p}_{\Psi_n}$. For Fréchet distance [7] calculation, points positions $\boldsymbol{p}_{\Phi_{\alpha(t)}}$, $\boldsymbol{p}_{\Psi_{\beta(t)}}$ are parameterized as a function of time $\alpha(t)$ and $\beta(t)$, $\alpha(t) : [0,1] \rightarrow \{1,2,...,n\}$ and $\beta(t) : [0,1] \rightarrow \{1,2,...,m\}$. Finding the Fréchet distance $D_F(\boldsymbol{p})$ requires finding the parameterizations of functions $\alpha(t)$ and $\beta(t)$ that minimize the maximum distance between inhalation and exhalation trajectories of a point $\boldsymbol{p}$:

$$D_F(\boldsymbol{p}) = \min_{\alpha(t),\beta(t)} \{ \max_{t\in[0,1]} d(\boldsymbol{p}_{\Phi_{\alpha(t)}}, \boldsymbol{p}_{\Psi_{\beta(t)}}) \}. \tag{2}$$

where $d(\boldsymbol{p}_{\Phi_{\alpha(t)}}, \boldsymbol{p}_{\Psi_{\beta(t)}})$ denotes the euclidian distance between points $\boldsymbol{p}_{\Phi_{\alpha(t)}}$ and $\boldsymbol{p}_{\Psi_{\beta(t)}}$. We make the assumption that over exhalation and inhalation, points have uniform motion. That is, $\alpha(t) = \beta(t) = k$. With this assumption, the Fréchet distance measure is simplified to the computation of the maximum distance between pairs of points $(\boldsymbol{p}_{\Phi_k}, \boldsymbol{p}_{\Psi_k})$:

$$Hyst_{\boldsymbol{p}} \approx \max_{k=1..n} d(\boldsymbol{p}_{\Phi_k}, \boldsymbol{p}_{\Psi_k}). \tag{3}$$

Figure 3 illustrates in 2D the hysteresis computation for two points trajectories for $n = 9$. We can notice with equation 3, that hysteresis is overestimated for some trajectory shapes. An exact hysteresis value could be computed if point velocity would be known for exhalation and inhalation. This would would allow us to calculate the functions of time $\alpha(t)$ and $\beta(t)$ for the Fréchet distance formula 2. We also evaluated the *relative hysteresis*, $R_{H/L}(\boldsymbol{p})$, which is the ratio between hysteresis and trajectory length for each point $\boldsymbol{p}$:

$$R_{H/L}(\boldsymbol{p}) = \frac{Hyst_{\boldsymbol{p}}}{L_{exh}(\boldsymbol{p}) + L_{inh}(\boldsymbol{p})} \tag{4}$$

We used the six regions cranio-caudal decomposition for lung point hysteresis evaluation. For each patient, we computed hysteresis in 3D as well as in the cranio-caudal, anterio-posterior, sagittal projection planes.

3 Results and discussion

Motion model In this work we generated a motion model by estimation of larger deformations between the end-exhale phase and all other states. Between 50 and 250 iterations of deformable registration were needed for one vector field estimation. For 1 million voxels, the computation time is about 1.5 seconds on a PC Pentium 4 (3.2 GHz, 2 Go Ram). We evaluated the accuracy and the consistency of the computed vector fields. Accuracy of vector fields was evaluated using control points. Approximately 60 points were selected for each patient and identified on each phase of the 4D-CT. Mean values (2.3 mm) of accuracy were on the order of the image resolution and comparable to inter-observer variability (1.9 mm). Vector fields were consistent, with close to zero (mean: 1.0 mm, standard deviation: 1.1 mm) mean and standard deviation values of the displacement vector norms of composite, $U_{XY} \circ U_{YX}$, deformation fields.

Motion non-linearity Motion model was used to analyze motion variations across the lung during the free-breathing cycle. First, we studied the non-linearity of the trajectory computed as the difference between the straight line trajectory and piecewise linear trajectories of exhalation and inhalation. The lungs were divided in six cranio-caudal regions for non-linearity and hysteresis evaluation. The upper side of the lung presented with very small non-linearity with maximum values comprised between 1.8 mm and 2.5 mm. The greatest non-linearity values were in the lower-middle regions of lung, with maxima situated in regions 4 or 5 (4.3 mm - 9.4 mm). The trajectory lengths also increase in the lower parts of the lung, which suggests that non-linearity is correlated with trajectory length. Trajectory lengths were greater over inhalation than for exhalation, but the difference was not statistically significant (p=0.19). The 4D-CT data used in this study was acquired from three patients presenting a diaphragmatic respiration. It was expected that the trajectory length would be greater in the lower regions of the lung. In future, it would be interesting to analyze data of patients with a thoracic respiration. We noticed the percentage of points with a non-linearity greater than the 2.5 mm slice thickness was small (only $\approx$ 5% of points for patient 1 and patient 3), except for patient 2 ($\approx$ 20%). This suggests that the trajectory between exhalation and inhalation could be approximated with a straight line for points with a non-linearity smaller than 2.5 mm. The non-linearity over inhalation and exhalation were significatively different for patient 1 (p=0.04)

and not significantly different for the two others (p=0.34 for patient 2 and p=0.1 for patient 3). We also evaluated how the 10% of points with highest non-linearity values were distributed inside the lungs. We noticed that the distribution is similar for the three patients: the major part of the points were situated in the lower-middle regions of lungs, which corresponds to regions containing the maximum values of non-linearity.

Motion hysteresis We observed common properties between the three patients: large hysteresis for second, third and fourth regions which correspond to lower-middle regions. Larger movement amplitudes were correlated with greater hysteresis values. The motion amplitude of patient 2 (6.6 mm average lung movement amplitude from end-exhale to end-inhale) is greater than for patient 1 (5.4 mm average lung movement amplitude from end-exhale to end-inhale) which is slightly greater than the motion amplitude of patient 3 (5 mm average lung movement amplitude from end-exhale to end-inhale). We were also interested to see how the 10% points with highest hysteresis were distributed inside lung. We noticed that they were situated in the lower-middle regions. Globally, we observed that hysteresis was directly related to trajectory lengths: a longer trajectory length implies greater hysteresis. We also evaluated the relative hysteresis, which is the ratio between hysteresis and trajectory length. We found different results compared with the absolute hysteresis: the upper-middle regions of the lung present small hysteresis, but a large relative hysteresis. The relative hysteresis values correlate with results obtained for the different regions of the lungs presented in [6]. Patient 2 had a large tumor situated in the right lower lobe with large displacement over the free breathing cycle: 14.6 mm average trajectory length over exhalation, and 17.6 mm average trajectory length over inhalation. We calculated a 14% average relative hysteresis for patient's 2 GTV which suggests that the major part of tumor displacement is not subject to hysteresis. The computation of this value with data from [6] gives comparable results: patients with large displacements of lower lobe lung tumors present a GTV relative hysteresis comprised between 4% and 16%.

4 Conclusion

In this study, we propose methods allowing to estimate and analyze patient specific organ deformations, and to compute some physiological parameters of motion over the free-breathing cycle. Here we studied 4D-CT data of only three patients. We introduced a motion model built from vector fields computed with deformable registration between the end-exhale state of a 4D-CT acquisition and all the other. The model was validated using consistency and accuracy metrics. The motion model was used for estimation and analysis of two physiological lung motion parameters, which are motion non-linearity and hysteresis. This makes possible inter-patient comparisons. For hysteresis estimation we introduced a measure inspired by Fréchet distance from computational geometry. The results demonstrated that motion trajectories can be nonlinear, and this nonlinearity varies across different regions within the lung. However, a straight line trajectory from end-exhale to end-inhale may be acceptable for some regions within the lung. Similarly, our results show that motion hysteresis varies across the lung. Hysteresis was found to be correlated with the total motion, having higher values in the lower regions of lungs.

In future, the integration of physiological information in a 4D lung atlas may have multiple clinical applications like analysis of inter-patient breathing, detection of specific (abnormal or not) breathing situations, and precise dosimetry study in radiotherapy.

References

[1] E. Rietzel, T. Pan, and G.T.Y. Chen. Four-dimensional computed tomography: image formation and clinical protocol. *Med. Phys.*, 32(4):874–89, 2005.

[2] J.P. Thirion. Image matching as a diffusion process: An analogy with maxwell's demons. *Medical Image Analysis*, 2(3):243–260, 1998.

[3] A. E. Lujan, J.M. Balter, and R.K. Ten Haken. A method for incorporating organ motion due to breathing into 3D dose calculations. *Med. Phys.*, 26(5):715–20, 1999.

[4] D.A. Low, P.J. Parikh, W. Lu, J.F. Dempsey, S.H. Wahab, J.P. Hubenschmidt, M.M. Nystrom, M. Handoko, and J.D. Bradley. Novel breathing motion model for radiotherapy. *Int. J. Radiat. Oncol. Biol. Phys.*, 63(3):921–9, 2005.

[5] G.S. Mageras and E. Yorke. Deep inspiration breath hold and respiratory gating strategies for reducing organ motion in radiation treatment. *Semin. Radiat. Oncol.*, 14(1):65–75, January 2004.

[6] Y. Seppenwoolde, H. Shirato, K. Kitamura, S. Shimizu, M. van Herk, and J.V. Lebesque. Precise and real-time measurement of 3D tumor motion in lung due to breathing and heartbeat, measured during radiotherapy. *Int. J. Radiat. Oncol. Biol. Phys.*, 53(4):822–34, 2002.

[7] H. Alt and M. Godau. Computing the Fréchet distance between two polygonal curves. *Internat. J. Comput. Geom. Appl.*, 5(1-2):75–91, 1995.